Surface & Coatings Technology 417 (2021) 127208

Contents lists available at ScienceDirect

Surface & Coatings Technology

journal homepage: www.elsevier.com/locate/surfcoat

Self-healing performance and corrosion resistance of novel CeO_2-sealed MAO film on aluminum alloy

Yue Gong [a,b], Jiwei Geng [a,b], Jie Huang [a], Zhe Chen [b], Mingliang Wang [a,b,*], Dong Chen [b,c,**], Haowei Wang [a,b]

[a] State Key Laboratory of Metal Matrix Composites, Shanghai Jiao Tong University, China
[b] School of Materials Science & Engineering, Shanghai Jiao Tong University, Shanghai, China
[c] Anhui Aluminium Matrix Composites Engineering Research Centre, Huaibei, China

ARTICLE INFO

Keywords:
Al alloy
Micro-arc oxidation
Corrosion inhibitor
Corrosion resistance
Self-healing

ABSTRACT

The self-healing performance with the improved corrosion resistance of novel CeO_2-sealed micro-arc oxide (MAO) film on Al alloy was studied in this work for the first time. There are three steps involved, including: (1) Preparing porous film by performing MAO treatment on Al alloy with the average thickness of ~15 μm; (2) loading corrosion inhibitor by soaking MAO sample in $Ce(NO_3)_3$ solution to fulfill micropores-sealing process; (3) evaluating the self-healing ability of the sealed MAO film in acidic, alkaline and neutral solutions by scratch tests. The experimental results indicated that the corrosion inhibitor was characterized to be CeO_2 which can locally fill the micropores to seal the MAO film. The optimized CeO_2-sealed MAO film owned the lower porosity and the improved the corrosion resistance, which can be testified from the corrosion current density (I_{corr}) decreased by 2 orders of magnitude compared with the MAO film. Furthermore, the micropores in the MAO film acted as microcontainers to hold corrosion inhibitor to make CeO_2-sealed MAO film showed self-healing ability. In the acidic environment (pH = 2 (8 mL/L H_2SO_4 + 20 mL/L H_2O_2)), the novel CeO_2-sealed film exhibited positive self-healing effect morphologically with improved corrosion test result, and the underlying self-healing mechanism was discussed in detail.

1. Introduction

Nowadays, the annual output of Al alloy is only second to the iron & steel in the metallic materials to meet the demand of lightweight tendency for structural materials [1]. Due to their lower density, higher specific strength and higher specific stiffness, Al alloys are widely used in the civilian field and aerospace fields [2–4]. For example, the high strength 7085 Al alloy with low quenching sensitivity can be used to manufacture the wing girders and wing auxiliaries of Airbus A380 [5–7]. However, its wider application has been hindered by the high chemical activity and low corrosion resistance of Al alloy [8]. Many surface treatments, i.e., thermal spraying [9,10], physical vapor deposition [11,12], chemical vapor deposition [13], and laser cladding [14–16], have been used to improve the corrosion resistance of Al alloy. These methods can improve the corrosion resistance of Al alloy in different degrees, and thus to increase its industrial utilization. Practically, the survey shows that Al alloy workpiece after surface treatment may occasionally be destroyed in the process of transportation or application [17–19]. Once the surface film is destroyed, the substrate can be vulnerable to local corrosion, leading to the film falling off and the failure of the Al alloy workpiece. The research on self-healing film [20] aims to address this problem, which is supposed to prevent the occurrence and further expansion of corrosion behavior in damaged areas on the Al alloy.

Self-healing film has attracted the researchers` attention in recent years owing to its intelligent repair ability [21,22]. Initially, it is a transformation film with the self-healing effect that introduces the corrosion inhibitor into the surface film. Moreover, the corrosion resistance of the film can be repaired by inhibiting the corrosion on the substrate once the film is destroyed [23,24]. Currently, the self-healing options include chemical conversion coating [25], doped self-healing coating [26] and microcontainer self-healing film [27]. Among these methods, the chemical conversion coating is the initial strategy which has received intensive interests. Herein, the heavy chromate conversion

* Correspondence to: M. Wang, School of Materials Science & Engineering, Shanghai Jiao Tong University, Shanghai, China.
** Correspondence to: D. Chen, Anhui Aluminium Matrix Composites Engineering Research Centre, Huaibei, China.
E-mail addresses: mingliang_wang@sjtu.edu.cn (M. Wang), chend@sjtu.edu.cn (D. Chen).

https://doi.org/10.1016/j.surfcoat.2021.127208
Received 17 February 2021; Received in revised form 13 April 2021; Accepted 17 April 2021
Available online 21 April 2021

coating, as a typical of chemical conversion coating, has good self-healing capability, mainly because the Cr(VI) oxide and the Cr(III) oxide are the main components of the conversion coating [28]. If the film is damaged, the Cr(VI) ion in the film can be released to form Cr_2O_3 and $Cr(OH)_3$ over the damaged area to inhibit its further corrosion occurrence [29]. However, the chromate has been banned because of its toxicity, which can do serious harm to humans and the environment. Therefore, there are many studies on the novel chemical conversion coating to replace the chromate. For example, Yoganandan et al. [30] prepared Zr&Ce conversion coating on the surface of 2024 Al alloy to study its self-healing ability. The corrosion resistance of samples soaked in 0.6 M NaCl solution for 168 h was slightly better than that soaked for 1 h. The Zr&Ce conversion coating showed self-healing effect, although the effect was weak due to the fewer content of the corrosion inhibitor in this coating.

Recently, the microcontainer self-healing film has gained increasingly investigations, such as nano-capsules [31], microvascular networks [27] and porous materials [32]. Normally, the preparations of nano-capsules and microvascular networks are considered complex. In regard to porous material, the micropores in the material can act as the natural microcontainers. In porous film, micropores can hold corrosion inhibitor, and the inhibitor fills the pores to seal the film. There are typically two steps involved to prepare porous self-healing film, i.e., (1) To fabricate a porous protective film on the metals. Herein, both anodic oxidation [33] and micro-arc oxidation (MAO) [34] methods can produce a layer of porous film on the metal surface to increase the corrosion resistance. The MAO method, as an environment friendly method, has exhibited its advantages on the higher hardness and improved corrosion resistance for the surface film [35]. As a result, the MAO treatment is more popular on the metals for the corrosion protection currently. (2) To load corrosion inhibitors in the porous film. Normally, the micropores of MAO film are desired as carriers of inhibitors. For example, there are available reports based on the MAO method on Mg alloys to load corrosion inhibitors to make the self-healing MAO film. Gnedenkov et al. [36] added organic corrosion inhibitor (8-hydroxyquinoline) into the MAO film on Mg alloy, and found that both corrosion resistance and self-healing performance were improved hereby in the neutral NaCl solution. Liu et al. [37] added both organic (2-mercaptobenzothiazole) and inorganic corrosion inhibitors (Na_3PO_4) to the MAO film on Mg alloy, and this duplex composite coating showed self-healing properties in the neutral NaCl solution by exerting their synergistic effects.

To expand the application of Al alloy, it is crucial to improve its corrosion resistance or induce its self-healing ability. However, there are rarely researches on self-healing MAO film for Al alloy. Furthermore, the work related to the self-healing film on alloys in the acidic and/or alkaline environments is also rare. Different from the chromate based solution, the Cerium-based solution has been reported to introduce the corrosion inhibitor on Al alloys [38]. Therefore, the Cerium-based corrosion inhibitor has a chance to fill the pores in the MAO film. Therefore, this work studied the self-healing film based on the MAO film on the 7085 Al alloy loaded with the corrosion inhibitor by soaking in $Ce(NO_3)_3$ solution. For the first time, we investigated the self-healing performance of such novel film in acidic, alkaline and neutral environments. Thus, a method to repair the damaged MAO film of Al alloy can be provided.

2. Experimental details

2.1. Materials

The as-cast 7085 Al alloy (Zn: 7.46 wt%, Mg: 1.63 wt%, Cu: 1.61 wt %, Zr: 0.15 wt% and Al balance) used in this experiment was home-made, and the elemental compositions were investigated via inductively coupled plasma mass spectrometry (ICP-AES) technique. At the beginning, the as-cast alloy was cut to make Φ 30 mm × 5 mm alloy sample. These samples were mechanically polished to a smooth surface by 80#, 180# and 400# SiC sandpaper in turn, washed with ethanol and deionized water, and dried in cold air finally.

2.2. Micropores sealing process

An AC power supplier (WHD-30) was utilized in the MAO experiment, in which the alloy sample was working as the anode, and the stainless-steel plate working as the cathode. The electrolyte used for the MAO treatment was the traditional silicate electrolyte, including 10 g/L $Na_2SiO_3{\cdot}9H_2O$, 2 g/L NaOH and 2 g/L EDTA. During the MAO process, the constant pressure mode was performed with the forward voltage was 350 V, and the negative voltage was 60 V. The voltage rose from 0 V to 350 V within 55 s at a rate of 6.4 V/s, and remained 350 V until the end of the reaction, which lasted for 15 min. During the MAO experiment, the electrolyte temperature was kept below 30 °C using an external circulation cooling system. After the MAO treatment, the sample was washed with deionized water at room temperature and dried with a hair dryer. Furthermore, the MAO treated alloy sample with porous film on its surface was named as the "MAO sample" for clarity. Tested by the ED400 Type EDDY current gauge, the average film thickness in the MAO sample was ~15 μm under this condition.

The MAO samples were impregnated in the $Ce(NO_3)_3$ solution to make the micropores-sealing process. This solution was prepared by the dissolution of $Ce(NO_3)_3$ and H_2O_2 in deionized water at 20 °C with the constant mechanical stirring. The $Ce(NO_3)_3$ content and H_2O_2 dosage in the solution were 6 g/L and 30 mL/L, respectively. Moreover, these MAO samples were soaked for certain durations to load the corrosion inhibitor, which can also fulfill the micropores-sealing process, accordingly. After the sealing treatment, these samples were washed with deionized water, and dried in the air. The MAO sample treated by the Micropores-Sealing process was named as the "Sealing sample" for convenience. For the Sealing sample, the sealed film which was made up of the porous film with the corrosion inhibitor inside. The whole experimental process is shown in Fig. 1.

2.3. Self-healing performance

In order to characterize the self-healing properties of sealed films in the Sealing samples in acidic, alkaline, and neutral solutions, each Sealing sample with an artificial scratch was immersed in acidic solution (pH = 2 (8 mL/L H_2SO_4 + 20 mL/L H_2O_2)), alkaline solution (pH = 13 (4 g/L NaOH)) and neutral solution (pH = 7 (36 g/L NaCl)) to simulate the damage of Al alloy workpieces during the service life, accordingly. A 17 mm (length) × 100 μm (width) scratch was made on the film surface with a turning tool. It was observed with an optical microscope to ensure that the scratch reached the Al substrate.

2.4. Materials characterizations

The SJ410 surface roughness meter was used to measure the surface roughness of the MAO and the Sealing samples. In order to ensure accuracy, the roughness of each sample was measured five times to obtain the average value. Besides, the porosity of the films for the MAO and the Sealing samples was measured by ImageJ software.

The Scanning Electron Microscopy (SEM, MIRA 3 XMH, TESCAN) equipped with the Energy-dispersive X-ray Spectroscopy (EDS) facility was used to observe the morphologies of the films for the MAO sample, Sealing sample and the Sealing sample after self-healing treatment. Furthermore, the element distribution on the Sealing sample surface was detected. It is necessary to conduct gold spraying treatment to enhance the electrical conductivity of these sample surfaces before SEM observation. The gold spraying treatment was made on the type MSP-1S vacuum gold spraying machine.

The X-ray Diffractometer (XRD, D8 ADVANCE Da Vinci) was used to detect the phase compositions of the studied samples with the 2θ range from 10° to 90° at a scanning rate of 2°/min. The X-ray Photoelectron

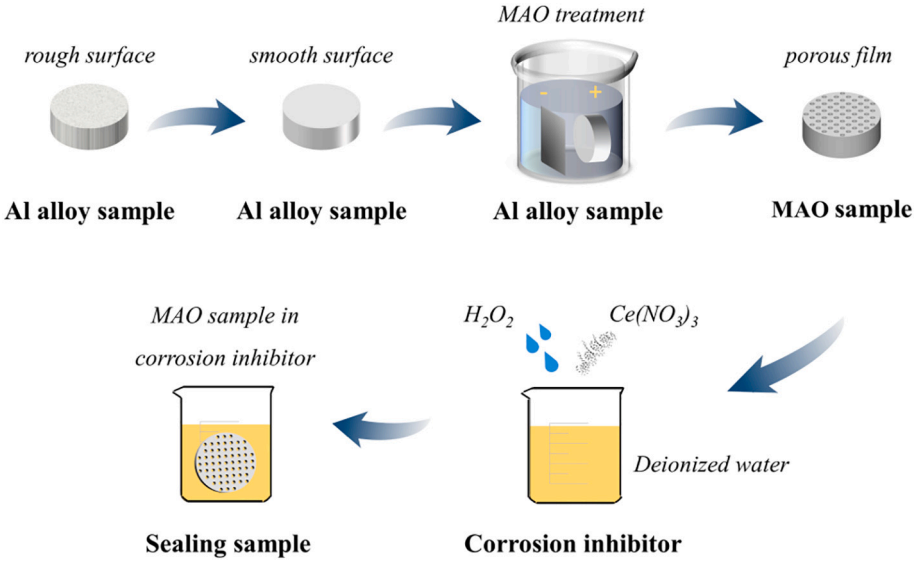

Fig. 1. Schematic diagram of the alloy sample treated by the MAO and micropores sealing processes.

Spectroscopy (XPS, Thermo Scientific K-Alpha) with the use of Al Kα radiation was utilized to probe the film composition for the Sealing sample and the self-healing product over the scratched area of the film, after they were immersed in acidic, alkaline and neutral solutions.

The CHI660C electrochemical workstation (Shanghai Chenhua) was employed to test the Potentiometric Polarization and Electrochemical Impedance Spectrum (EIS) to characterize the electrochemical features of the samples. In detail, the sample was immersed in 3.5 wt% NaCl solution with an exposed surface area of 1 cm^2. A typical three-electrode device was used with the sample as the working electrode, the saturated calomel electrode as the reference electrode, and the platinum electrode as the counter electrode. In order to obtain a stable Open Circuit Potential (OCP), the immersion time was 30 min. The Electrochemical Impedance Spectroscopy measurement was carried out with the frequency ranged from 0.1 Hz to 10^5 Hz, and the amplitude was 10 mV. In the determination of potentiometric polarization curve, the scanning speed was set to be 30 mV/min. In order to ensure the accuracy of the experimental results, three parallel tests were conducted.

3. Results and discussions

3.1. Micropores-sealing behavior

3.1.1. Macroscopic morphology observation

Four MAO samples are immersed in the $Ce(NO_3)_3$ solution for different durations to perform the sealing treatment. In detail, there are four soaking durations (i.e., 10, 30, 60 and 90 min) to make four Sealing samples, accordingly. The macroscopic morphologies of one MAO

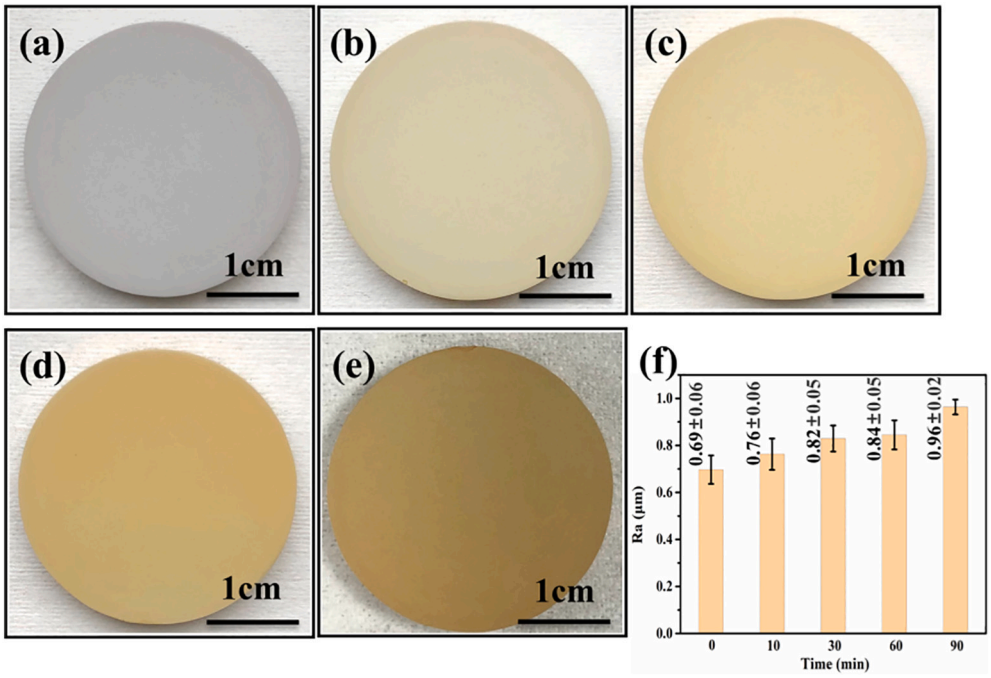

Fig. 2. Macroscopic morphologies of the MAO sample (soaking for (a) 0 min) and the four Sealing samples (soaking for (b) 10, (c) 30, (d) 60 and (e) 90 min); (f) surface roughness of the MAO sample and the four Sealing samples.

sample and four Sealing samples are presented in Fig. 2(a–e), where the color changes of these samples are clearly observed, accordingly. Obviously, the colors of these samples are gradually deepened and turn from gray white (MAO sample without soaking treatment) to yellow brown with the increase of soaking time. It is well known that the Ce^{4+} ions can make the solution or compound show the yellow based appearance [39]. Therefore, it is reasonable to infer that the corrosion inhibitor should be gradually formed inside the MAO films, and be related to the Ce^{4+} based compound with the increasing soaking duration.

Furthermore, the surface roughness of one MAO sample and four Sealing samples can be elevated with the prolonging soaking duration (Fig. 2(f)). This evidence should be correlated with the higher amount of formed corrosion inhibitor with the extension of soaking time.

3.1.2. Surface morphology observation and chemical composition analysis

The surface morphologies of MAO sample (Sealing-0 min sample), Sealing-60 min sample and Sealing-90 min sample are shown in Fig. 3 (a–c), accordingly. For the Sealing-0 min sample, the number and the size of micropores in its sealed film are both larger (Fig. 3(a)). Specifically, the porosity of this film is measured to be 3.06% (Fig. 3(f)). For the Sealing-60 min sample, the surface morphology is obviously different from that of the MAO sample, and the porosity of the sealed film has decreased to 1.57% (Fig. 3(f)). When the MAO sample sealed for 90 min, more obvious cracks appeared on the surface in the Sealing-90 min sample (Region C in Fig. 3(c)). Correspondingly, the porosity of Sealing-90 min sample has increased to 1.84% (Fig. 3(f)). It seems the porosity does not decrease all the time with the increase of soaking time, indicating that the soaking efficiency for the formation of corrosion inhibitor changes in a near parabolic pattern.

Fig. 3(d) exhibited an enlarged image of region A, the micropores boundary in the MAO film (Sealing-0 min sample) is smooth and clear, which is different from the micropores morphology in the Sealing-60 min sample (Fig. 3(e)). To clarify the dispersion state of corrosion inhibitor in the sealed film, the EDS elemental mapping of the Sealing-60 min sample has been carried out on its surface. The elements distributions of Al, Ce and O elements are reflected in Fig. 3(g–i), accordingly. Notably, Al (Fig. 3(g)) and O (Fig. 3(i)) are uniformly distributed on the surface, indicating that Al_2O_3 is the main phase of the film in Sealing sample. It is interesting to found that the micropores indicated by the arrows and dotted lines in Fig. 3 (e) are the Ce-rich regions (Fig. 3(h)), which means that the Ce-based compound can locally fill the micropores to seal MAO film under capillary action, which illustrates that the micropores of the MAO film can act as microcontainers to hold corrosion inhibitor.

In order to figure out the corrosion inhibitor in the Sealing sample, the chemical composition of this sample has been characterized by XRD and XPS characterization methods. Fig. 4(a) presents the XRD pattern of the Sealing-0 min sample and Sealing-60 min sample. Both samples have shown to be composed of γ-Al_2O_3 and α-Al_2O_3, without any significant difference in phase composition. To further determine the corrosion inhibitor in the sealed film, XPS analysis is adopted. The high-resolution spectra of Ce 3*d* (Fig. 4(b)) and O 1*s* (Fig. 4(c)) are exhibited. Fig. 4(b) displays that Ce 3*d* peak signal is rarely detected in the Sealing-0 min sample, while the Sealing-60 min sample shows the obvious Ce 3*d* peak. It implies that the corresponding compounds have been created into the Sealing samples successfully. In detail, the Ce 3*d* spectrogram of the Sealing-60 min sample is fitted by peak fitting, and the original

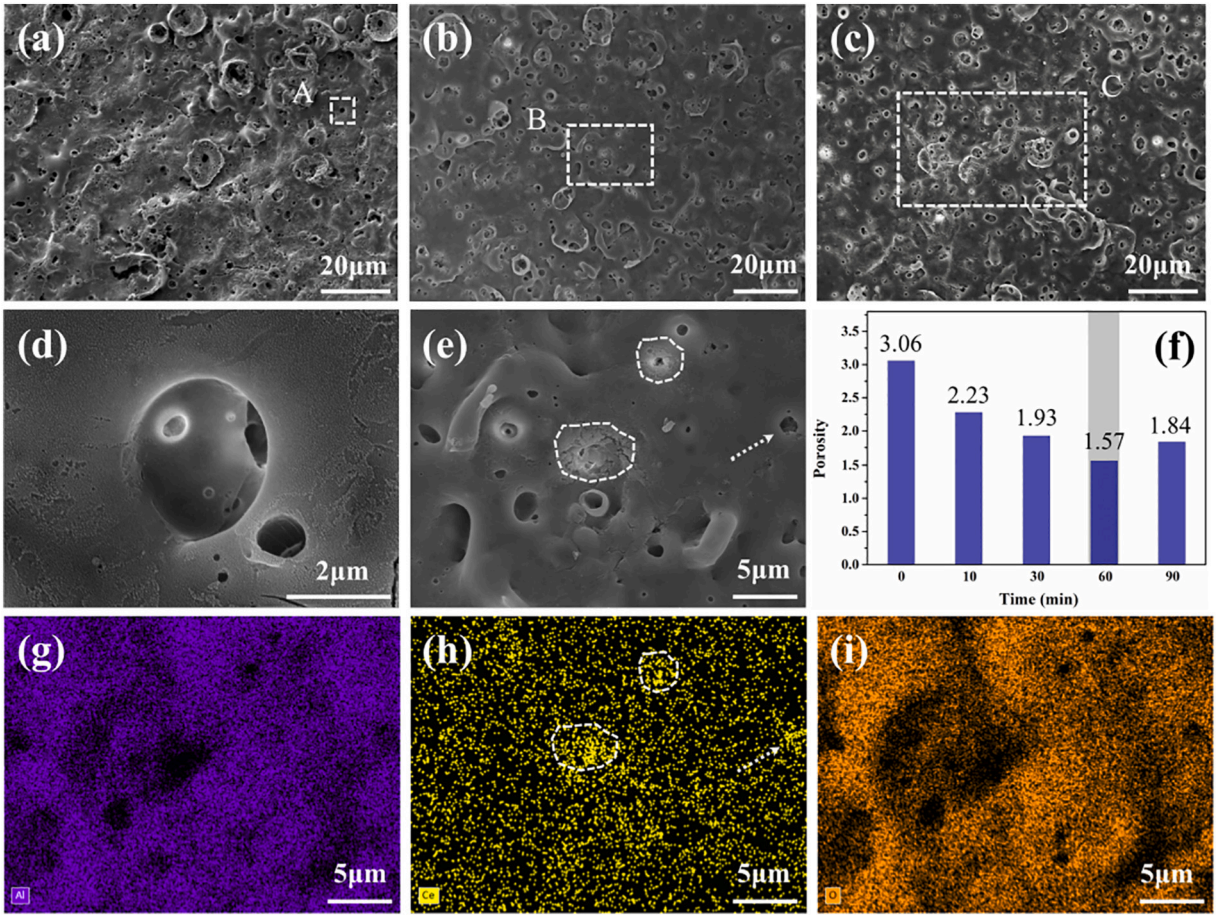

Fig. 3. Surface morphologies of the MAO sample (soaking for (a) 0 min) and the Sealing samples (soaking for (b) 60, (c) 90 min), (d) enlarged image of region A, (e) enlarged image of region B; (f) porosity of the MAO sample and the four Sealing samples; the EDS elemental mapping of region B: (g) Al map; (h) Ce map; (i) O map.

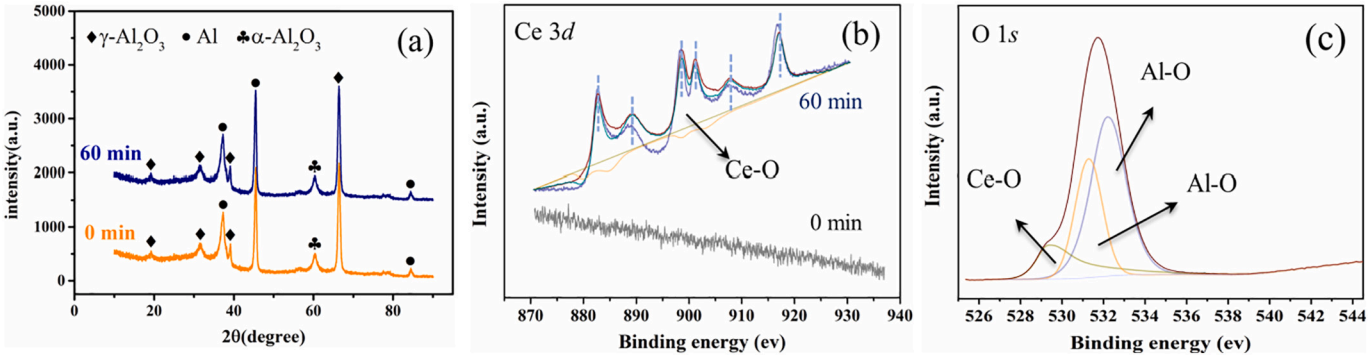

Fig. 4. (a) XRD spectra of the Sealing-0 min sample and Sealing-60 min sample; XPS spectra of the Sealing-60 min sample (b) Ce, and (c) O.

spectrogram is found to be highly consistent with the standard spectrogram of Ce $3d^{4+}$, which demonstrates that the corrosion inhibitor in the Sealing sample contains Ce $3d^{4+}$. The XPS peaks at the binding energies of ~882.7 eV, 881.8 eV, 898.3 eV, 900.8 eV, 907.3 eV and 916.7 eV represent the existence of CeO_2 [40,41] in the Sealing sample. Fig. 4 (c) illustrates that the peak of O 1*s* peak can be divided into 3 peaks. Determined by comparison with NIST database, the peaks at the binding energies of ~531.3 eV, 532.2 eV corresponding to Al_2O_3 [42,43] and 529.4 eV corresponding to CeO_2 [44], accordingly. Therefore, it can be concluded that the phase composition of the film in the MAO sample is γ-Al_2O_3 and α-Al_2O_3, and the corrosion inhibitor created in the sealed film of the Sealing sample is CeO_2. The related chemical reactions are suggested thereafter.

The $Ce(NO_3)_3$ solution used to seal the micropores in the MAO sample is orange. Because the H_2O_2 addition can cause the oxidation of $Ce(NO_3)_3$, this should convert the Ce^{3+} ions to Ce^{4+} ions following the chemical reaction (Eq. (1)). Since the amount of H_2O_2 in the corrosion inhibitor solution has far exceeded the required H_2O_2 amount for the completed oxidation of Ce^{3+} ions, the Ce element should mainly exist as Ce^{4+} ions before the sealing treatment.

When the MAO sample is immersed in the $Ce(NO_3)_3$ solution, the reduction of molecular oxygen is a major electrochemical mechanism of the sealing process, in which O_2 is reduced to OH^- via a direct four-electron reduction path way [45] according to Eq. (2). Subsequently, the solution pH increases with the elevating OH^- ions concentration. Especially, the higher local pH value on the surface of MAO film can induce the reaction around micropores (Eq. (3)). Thereby, CeO_2 is formed around or inside the micropores, and seals the porous film indeed. However, the created OH^- ions (Eq. (2)) probably have dissolving effects on the alumina-based MAO film, and thus to degrade the integrity and corrosion resistance of samples in the over-longed sealing treatment.

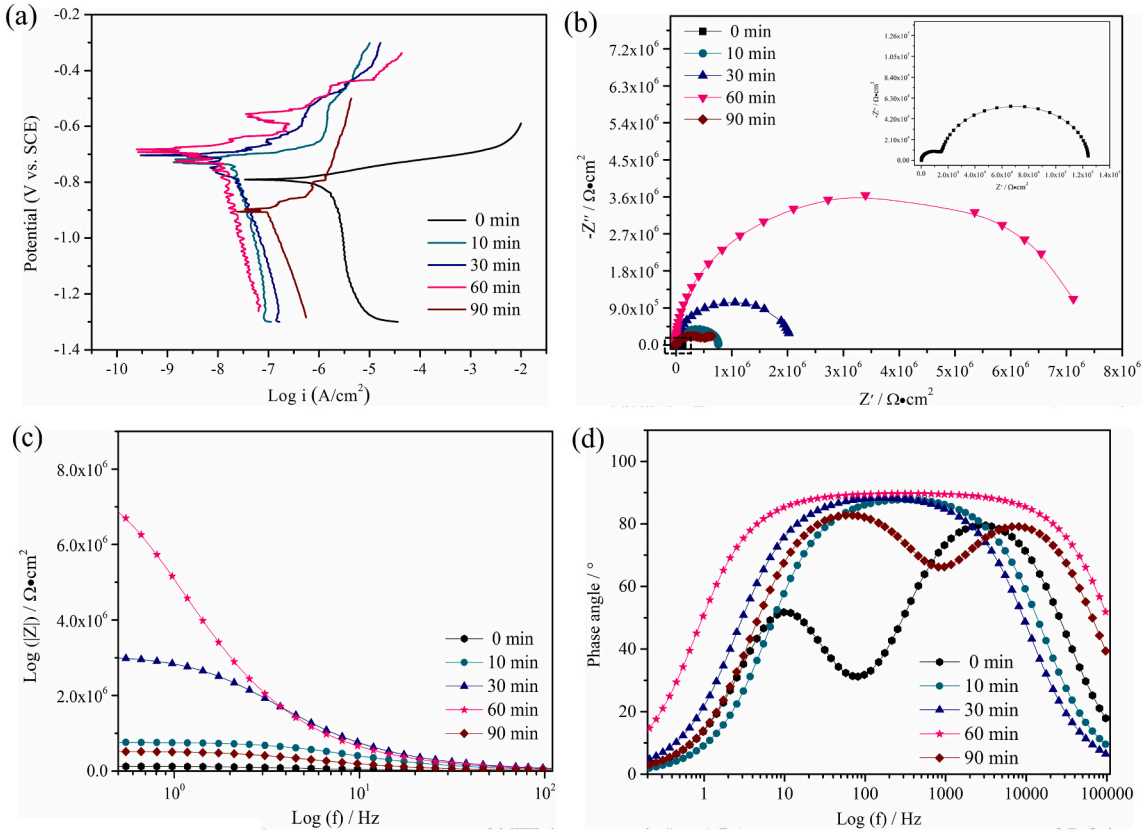

Fig. 5. (a) Potentiometric polarization curves, (b) Nyquist plot with a high magnification inset, (c) Bode impedance plot, (d) Bode phase plot for the MAO sample (soaking for 0 min) and the four Sealing samples (soaking for 10, 30, 60 and 90 min).

$$2Ce^{3+} + H_2O_2 + 2H_2O \rightarrow 2Ce(OH)_2^{2+} + 2H^+ \quad (1)$$

$$2H_2O + O_2 + 4e^- \rightarrow 4OH^- \quad (2)$$

$$Ce(OH)_2^{2+} + 2OH^- \rightarrow Ce(OH)_4 \rightarrow CeO_2 + 2H_2O \quad (3)$$

Combined with the above analysis, it has concluded that the Ce $(NO_3)_3$ has the ability to seal the micropores of the MAO film by the formation of CeO_2 compound in these pores.

3.1.3. Electrochemical measurements

From the morphological observation, the corrosion inhibitor has shown sealing effect on the micropores. Then, the electrochemical behavior is further studied to evaluate the corrosion resistance of CeO_2-sealed MAO film for the Sealing sample. Potentiometric polarization curves employed to characterize the corrosion resistance of the Sealing samples (Fig. 5(a)). The corrosion current density (I_{corr}) is capable to reflect the corrosion resistance directly [46]. It is worth noting that there is an inverse relationship between I_{corr} and corrosion resistance. Among the MAO sample and the four Sealing samples, the I_{corr} of the Sealing-60 min sample is the most negative. Table 1 lists the fitting data of the polarization curves. Correspondingly, it is confirmed that the corrosion inhibitor is beneficial to improve the corrosion resistance of the MAO sample. When the sealing time is 60 min, the I_{corr} of the Sealing sample decreases by two orders of magnitude from 8.4×10^{-7} A·cm^{-2} to 6.4×10^{-9} A·cm^{-2} compared with the Sealing-0 min sample, which indicates that the corrosion resistance of the MAO sample is significantly improved. In addition, the corrosion voltage (E_{corr}) also expresses the similar rule with the I_{corr}.

The Nyquist plots of one MAO sample and four Sealing samples are shown in Fig. 5(b). In this case, it is found that the radii of these curves show the clear difference. Since the EIS results represent the corrosion behavior of the Sealing samples, the Nyquist curve with a larger radius indicates the improved corrosion resistance [47]. When the immersion time is from 0 to 60 min, the radii of the curves gradually increase with the increasing soaking time. It has thus signified that the corrosion resistances of these Sealing samples gradually increase. This change also implies that the charge transfer process is inhibited, and corrosion inhibitors are effectively loaded into the MAO films [48]. More ions have entered the MAO film, and more corrosion inhibitors are formed with the extension of soaking time, leading to the gradual improvement of sealing effect. The corrosion resistance appears a downward trend when the soaking time is 90 min. This phenomenon should be inclined to be attributed to the dissolving effect on the CeO_2-sealed film has dominated in the sealing duration.

Furthermore, the Bode impedance plot and phase plot of one MAO sample and four Sealing samples are shown in Fig. 5(c) and (d), respectively. In the low frequency region, the film with a higher Z modulus (|Z|) always has a better corrosion resistance. It is evident that the Sealing-60 min sample shows the best corrosion resistance owing to its higher Z modulus (Fig. 5(c)). Analyzed from Fig. 5(d), two-time constants can be found in the spectra of the films in MAO sample and Sealing-90 min sample, and one-time constant is found in the spectrum of the other Sealing samples (soaking for 10, 30, and 60 min). The equivalent electrical circuits are fitted by the EIS data of MAO sample (Fig. 6(a)), Sealing samples (soaking for 10, 30, and 60 min) (Fig. 6(b)),

Table 1
Polarization fitting results of the MAO sample (soaking for 0 min) and the four Sealing samples (soaking for 10, 30, 60 and 90 min).

Sample	β_a/mV·dec^{-1}	$-\beta_c$/mV·dec^{-1}	I_{corr}/A·cm^{-2}	E_{corr}/V	R_p/Ω·cm^2
0 min	2.84	42.54	8.4E-07	−0.795	1.6E4
10 min	18.86	35.64	3.8E-08	−0.734	4.7E5
30 min	9.86	10.28	1.2E-08	−0.767	3.1E6
60 min	2.51	11.32	6.4E-09	−0.674	6.5E6
90 min	14.11	41.15	1.9E-07	−0.941	3.2E5

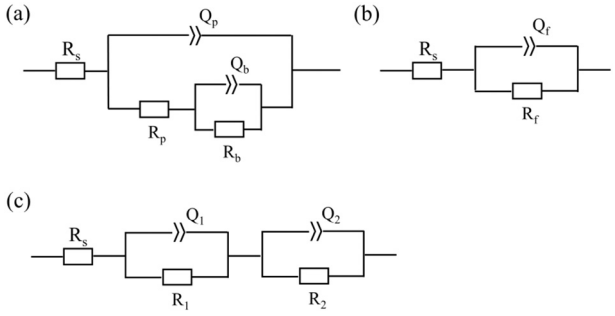

Fig. 6. Equivalent electrical circuits used for fitting the EIS data of (a) MAO sample, (b) Sealing samples (soaking for 10, 30, and 60 min), (c) Sealing-90 min sample. R_s: the resistance of the solution, R_p: the resistance of the porous layer, R_b: the resistance of the barrier layer, Q_p: the capacitance of the porous layer, Q_b: the capacitance of the barrier layer, R_f: the resistance of the sealed film, Q_f: the capacitance of the sealed film, R_1: the resistance of the film, R_2: the resistance of the interface between film and substrate, Q_1: the capacitance of the film, Q_2: the capacitance of the interface between film and substrate.

and Sealing-90 min sample (Fig. 6(c)). R_s refers to the resistance of the solution. As a common sense, the MAO film consists of an outer porous layer and an inner compact layer [49]. Therefore, R_p and R_b in (Fig. 6(a)) refer to the resistance of the porous layer and barrier layer, respectively; Q_p and Q_b refer to the capacitance of the porous layer and barrier layer, respectively. The equivalent electrical circuit model with constant phase angle element (Q) is usually adopted in the electrolyte section to replace capacitor [50]. Q is used to describe the physical quantity in which the parameter of capacitance is deviated. It is related with two variables, i.e., Y (admittance, the reciprocal of impedance) and n (phase factor). If $n = 1$, Q = C (capacitor). The parameters derived from the corresponding equivalent electrical circuit models are listed in Table 2.

The Bode phase plot of the Sealing samples (soaking for 10, 30, and 60 min) only shows one-time constant, it must because that the corrosion inhibitors are introduced into the MAO film successfully. The corrosion resistance of porous layer is improved and the invasion of corrosive medium is effectively suppressed. When the soaking time reaches to 90 min, the Sealing-sample shows poor corrosion resistance, the Bode phase plot of the Sealing-90 min sample reveals two-time constants again. Combined with the observation of morphology in Fig. 3(c), the long-time immersion in $Ce(NO_3)_3$ causes more cracks on the surface of the MAO film, which accelerates the corrosion reaction.

Conclusively, both electrochemical measurements and SEM morphologies can demonstrate that the corrosion resistance of the MAO film can be improved by the micropores sealing process. Moreover, the corrosion resistance reaches its best for the CeO_2-sealed film when the sealing time is 60 min.

3.2. Self-healing performance

3.2.1. Self-healing morphology and electrochemical measurements

The Sealing-60 min sample with the best sealing effect is scratched to study its self-healing ability in acidic solution (pH = 2 (8 mL/L H_2SO_4 + 20 mL/L H_2O_2)), alkaline solution (pH = 13 (4 g/L NaOH)) and neutral solution (pH = 7 (36 g/L NaCl)). Specifically, the scratch morphologies of the parallel Sealing-60 min samples are to be self-repaired in acidic (Fig. 7(a1)), alkaline (Fig. 7(b1)) and neutral (Fig. 7(c1)) solutions are presented. Furthermore, the self-healing experiments are performed in acidic, alkaline and neutral solutions for 60, 30 and 120 min, accordingly. This is due to the corrosion behaviors of Sealing samples in the acidic, alkaline and neutral solutions are different. In consideration of the possible failure of sealed films, the appropriate self-healing time is ascertained in different environments.

Notably, Fig. 7(a2) exhibits that the scratch can be repaired effectively in the acidic solution, indicating that self-healing products are

Table 2
Parameters from equivalent electrical circuit model of MAO sample and the Sealing samples (soaking for 10, 30, and 60 min). The unit of resistance and capacitance is $\Omega \cdot cm^2$ and $F \cdot cm^{-2}$, respectively.

Sample	R_s	R_p	R_b	Q_p	n_p	Q_b	n_b	R_f	Q_f	n_f	R_1	R_2	Q_1	n_1	Q_2	n_2
0 min	117.1	5.9E3	1.4E4	9.7E−6	0.67	2.2E−7	0.8	–	–	–	–	–	–	–	–	
10 min	51.32							1.1E6	4.1E−7	0.73	–	–	–	–	–	
30 min	56.68							4.2E6	1.1E−7	0.8	–	–	–	–	–	
60 min	29.47							1.1E7	8.5E−8	0.87	–	–	–	–	–	
90 min	1.895	–	–	–	–	–	–	–	–	–	8.4E5	3.8E5	2.7E−6	0.68	1.3E−7	0.9

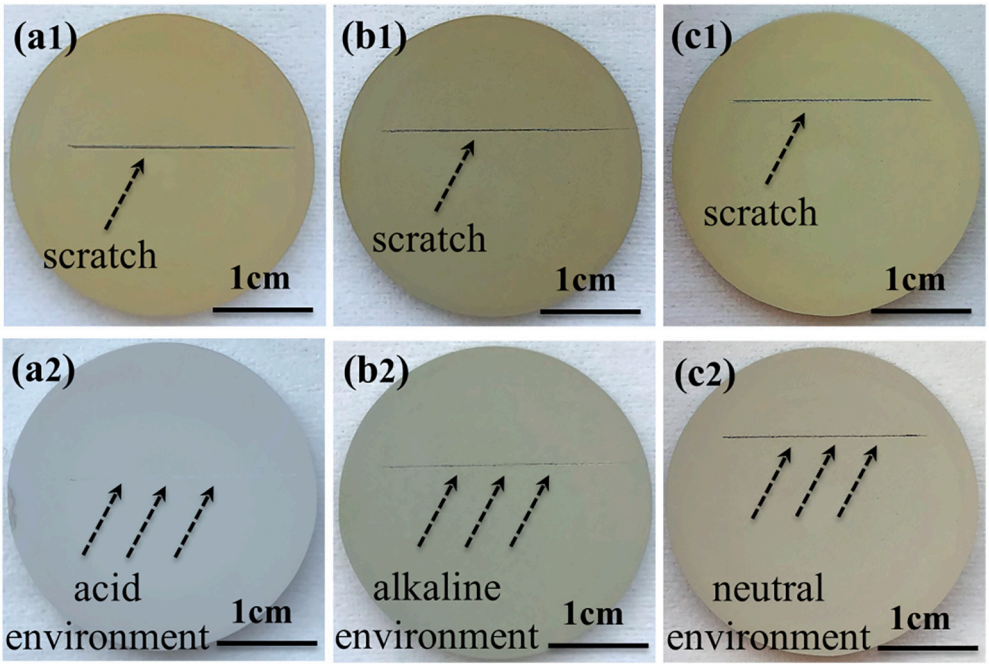

Fig. 7. Macroscopic morphologies of the scratches on the parallel Sealing-60 min samples (a1, b1, c1) before and (a2, b2, c2) after self-healing in acidic, alkaline and neutral solutions.

generated herein. In the alkaline solution (Fig. 7(b2)), a certain degree of repair is observed on the sample surface as well. Besides, there is hardly obvious repair morphology observed above the scratch in the neutral solution, as shown in Fig. 7(c2). Generally, it can be speculated from the macroscopic morphologies of the scratches that the CeO_2-sealed film in the Sealing-60 sample has a favorable self-healing effect in the acidic environment.

To observe the self-healing products, the microscopic morphologies of the scratches after the self-healing treatment in acidic (Fig. 8(b)), alkaline (Fig. 8(c)) and neutral (Fig. 8(d)) solutions are presented. Fig. 8 (a) shows the scratch on the Sealing-60 min sample without self-healing treatment. Unlike corrosion morphologies in Fig. 8(c) and (d), there are new self-healing products (indicated by the arrows) generated on the original scratch area (Fig. 8(b)). Comparably, the color of the scratch area turns black, and corrosion pit appears in alkaline solution (Fig. 8 (c)). Seriously, there are much more corrosion pits on the scratch area after the self-healing treatment in the neutral solution (Fig. 8(d)). Therefore, the appearance of corrosion morphology accounts for that the CeO_2-sealed film has little self-healing capability in alkaline and neutral solutions.

In order to further determine the self-healing effect, the electrochemical test is carried out on the scratch area. Fig. 9 illustrates the polarization curves of the scratches on Sealing-60 min samples with/without the self-healing treatment in different solutions. Combined with the polarization fitting results in Table 3, the I_{corr} above the scratched area without self-healing is 8.5×10^{-7} $A \cdot cm^{-2}$. Surprisingly, for the Sealing-60 min sample in acidic solution, the I_{corr} decreases by only ~1 order of magnitude to 5.3×10^{-8} $A \cdot cm^{-2}$. The improvement of corrosion resistance proves that the scratch is repaired effectively after self-healing treatment in acidic solution. Namely, the self-healing products observed in Fig. 8(b) should be conducive to the improvement of corrosion resistance, which ascertains that CeO_2-sealed film has self-healing capability in acidic environment. Comparably, the I_{corr} value increases by ~1 order of magnitude in alkaline and neutral solutions. These results manifest that the CeO_2-sealed films have rarely self-healing effect, and are severely corroded in both alkaline and neutral conditions.

3.2.2. *Self-healing process analysis*

Scratch areas are detected by XPS to confirm the components of self-healing products in different solutions (Fig. 10). Fig. 10(a) shows the peak fitting of element Ce 3*d*. Unexpectedly, the Ce 3*d* peak signal is hardly detected from the Sealing-60 min sample after the immersion in the acidic solution. It is probably because CeO_2 in the sealed film reacted with H_2SO_4 to form $Ce_2(SO_4)_3$ at first (Eq. (4)). Notably, $Ce_2(SO_4)_3$ is easily soluble in the aqueous solution.

$$2CeO_2 + H_2O_2 + 3H_2SO_4 = Ce_2(SO_4)_3 + 4H_2O + O_2\uparrow \quad (4)$$

In addition, the high-resolution spectrogram of O 1*s* is shown in Fig. 10(b). The O 1*s* peak of the Sealing-60 min sample after self-healing in acidic solution can be divided into two peaks, 531.4 eV for $Al(OH)_3$ [51] and 532.2 eV for Al_2O_3 [43]. This is because the Ce^{4+} ion has strong oxidation property under acidic condition which should oxidize H_2O_2 to give off O_2, leading to an increase in pH value. Thereby, the exposed Al

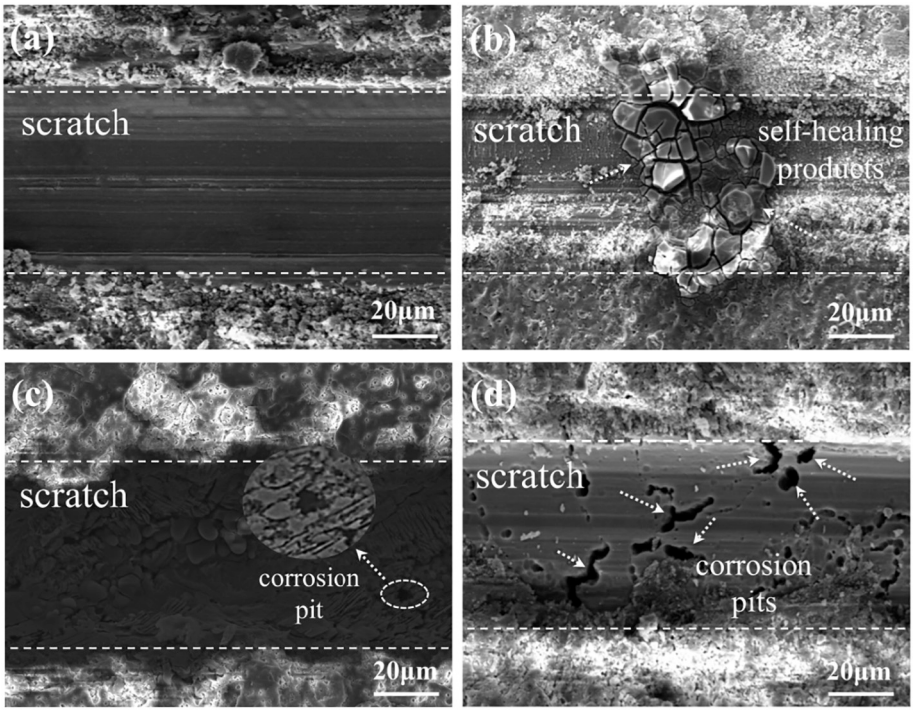

Fig. 8. Morphologies of the scratches on the parallel Sealing-60 min samples (a) without self-healing, after self-healing in (b) acidic, (c) alkaline, and (d) neutral solutions.

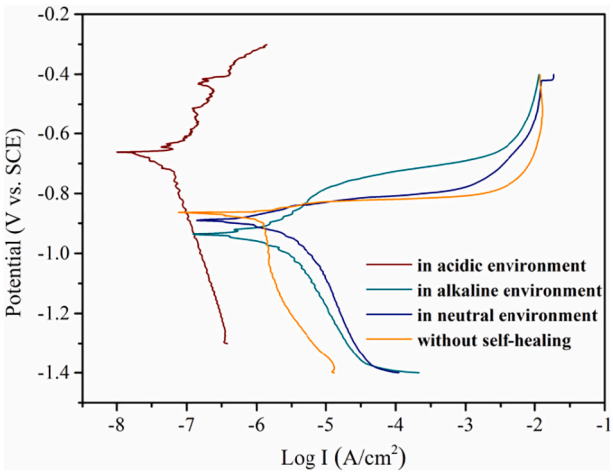

Fig. 9. Potentiometric polarization curves of the Sealing-60 min samples with/without self-healing in acidic, alkaline and neutral solutions.

Table 3
Polarization fitting results of the Sealing-60 min samples with/without self-healing in acidic, alkaline and neutral solutions.

Sample	β_a/mV·dec^{-1}	$-\beta_c$/mV·dec^{-1}	I_{corr}/A·cm^{-2}	E_{corr}/V
Acid	33.59	66.88	5.3E−08	−0.696
Alkaline	17.22	22.47	4.8E−06	−0.928
Neutral	2.41	21.66	2.1E−06	−0.853
Without healing	10.28	114.05	8.5E−07	−0.894

surface may be reacted with O_2 and H_2O to form $Al(OH)_3$ (Eq. (5)).

$$4Al + 3O_2 + 6H_2O = 4Al(OH)_3 \quad (5)$$

Interestingly, the CeO_2 peaks of the Sealing-60 min samples after self-healing in alkaline and neutral solutions are similar with the Sealing-60 min sample without scratching. It signifies that CeO_2 has not participated in the self-healing reaction under both circumstances. Treated by the alkaline solution, the XPS peaks of the Sealing-60 min sample are found to contain Al_2O_3, $NaAlO_2$ and CeO_2. The chemical reaction occurring in this environment is shown in Eq. (6).

$$A1_2O_3 + 2NaOH = 2NaAlO_2 + H_2O \quad (6)$$

Additionally, the peaks of the Sealing-60 min sample after self-healing in neutral solution are Al_2O_3 and CeO_2. According to the microscopic appearance of the scratch (Fig. 8(d)), a large number of corrosion pits appeared, which means that corrosion reaction must have occurred here. However, the corrosion product is yet detected by XPS. This is probably because the corrosion product related to $AlCl_3$ is soluble. In the environment of NaCl, Cl^- ions in the solution should be adsorbed on the surface to replace O^{2-} ions, thus forming $AlCl_3$ [52]. The structure of the CeO_2-sealed film is damaged, and corrosion pits are formed because $AlCl_3$ is easily soluble in water. Seriously, the corrosion pits should become the corrosion channel for harmful substances to erode the substrate, leading to a reduced corrosion resistance CeO_2-sealed film for the Sealing sample.

To describe a possible self-healing mechanism of CeO_2-sealed film, the self-healing process of the Sealing sample after self-healing in acidic environment is illustrated in Fig. 11. The whole process is divided into the following two parts: (1) CeO_2 can react with H^+ and H_2O_2 to release Ce^{3+} ions and O_2 molecules; (2) Al should react with O_2 and H_2O to form $Al(OH)_3$ to repair the film on the scratched area.

CeO_2 mainly exists in the outer porous layer of the MAO film, while the compact layer is mainly composed of $A1_2O_3$, as presented in Fig. 11 (a). Under the stimulation of acidic environment, CeO_2 should react with H^+ and H_2O_2 to release Ce^{3+} ions and O_2 molecules at the scratch area. Since the fact that the MAO film almost turns gray at the end of the self-healing process (Fig. 7(a2)), suggesting that CeO_2 has participated in the reaction thoroughly to release Ce^{3+} ions (Eq. (4)). In order to maintain the electronic balance of charge layer, cations in the solution are moving into the CeO_2-sealed film as indicated in Fig. 11(b) and (c). Sequentially, the exposed Al matrix at the scratch can react with O_2 and

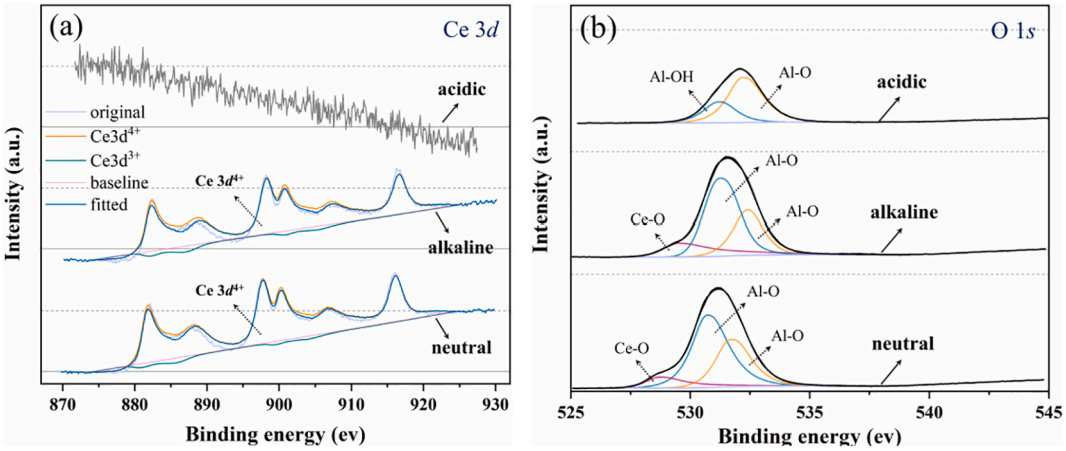

Fig. 10. XPS on the scratches for the parallel Sealing-60 min samples after self-healing in acidic, alkaline and neutral solutions: (a) Ce 3*d*; (b) O 1*s*.

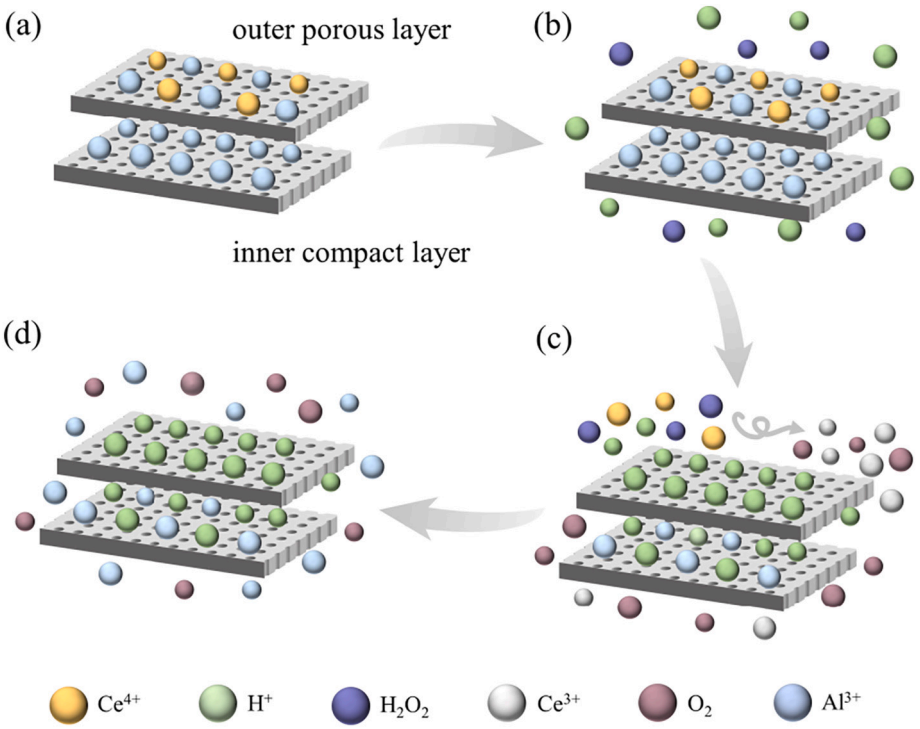

Fig. 11. Schematic diagram of self-healing mechanism in acidic environment.

H_2O in a locally oxygen-enriched solution to form a protective layer, thereby inhibiting further penetration of the corrosive medium, as presented in Fig. 11(d). This should be the reason for the difference in self-healing effect between acidic environment and other two environments.

4. Conclusion

In this work, the self-healing performance with the improved corrosion resistance of novel CeO_2-sealed MAO film on Al alloy was studied for the first time. Firstly, we have performed the MAO treatment on the 7085Al alloy. The porous film on the MAO film sample is prepared on the Al alloy, and the film has the average thickness of ~15 μm. Secondly, the micropores sealing process has been made on the MAO sample using the $Ce(NO_3)_3$ solution to induce the creation of corrosion inhibitor. Such inhibitor is characterized to be CeO_2 on the Sealing samples. Furthermore, it is found that the CeO_2 is locally enriched filling the microspores to seal the film, which illustrates that the micropores of the MAO film can act as microcontainers for holding corrosion inhibitor. When the micropores sealing process lasts for 60 min, the porosity of the CeO_2-sealed film is the lowest and the corrosion resistance is the best, which can be testified from the corrosion current density (I_{corr}) decreases by 2 orders of magnitude compared with the MAO sample without sealing treatment.

Finally, the scratch tests have been made on Sealing samples with the optimized corrosion resistance to evaluate the self-healing ability in acidic, alkaline and neutral solutions.

- In acidic environment (pH = 2 (8 mL/L H_2SO_4 + 20 mL/L H_2O_2)), the CeO_2-sealed MAO film has exhibited the positive self-healing effect morphologically with improved corrosion test result. Therefore, this method can provide an inspiration to repair the damaged MAO film of Al alloy, which normally occurs in the process of transportation or application.

- In alkaline environment (pH = 13 (4 g/L NaOH)), the scratch area presents a partially repaired macroscopic morphology, but the corrosion resistance of the CeO_2-sealed MAO film is not improved.
- In neutral solution (pH = 7 (36 g/L NaCl)), there is rarely self-healing effect generated in the CeO_2-sealed MAO film, and the corrosion pits are clear on the scratched surface.

The self-healing mechanism of the CeO_2-sealed film in acidic environment can be understood as the following two parts: (1) CeO_2 can react with H^+ and H_2O_2 to release Ce^{3+} ions and O_2 molecules; (2) Al should react with O_2 and H_2O to form $Al(OH)_3$ to repair the film on the scratched area of the surface.

CRediT authorship contribution statement

Yue Gong: Investigation, Validation, Writing-original draft. **Jiwei Geng:** Investigation, Resources, Formal analysis, Writing-review & editing. **Jie Huang:** Data curation, Formal analysis, Writing-review & editing. **Zhe Chen:** Data curation, Formal analysis, Writing-review & editing. **Mingliang Wang:** Conceptualization, Resources, Funding acquisition, Formal analysis, Writing-review & editing. **Dong Chen:** Conceptualization, Funding acquisition, Formal analysis, Writing-review & editing. **Haowei Wang:** Resources, Supervision, Writing-review & editing.

Declaration of competing interest

The authors declare that they have no known competing financial interests or personal relationships that could have appeared to influence the work reported in this paper.

Acknowledgments

The authors gratefully acknowledge the financial supports from by the National Natural Science Foundation of China (Grant No. 52071207), the China Postdoctoral Science Foundation (Grant No. 2019TQ0193, 2019M661497), the National Key Research and Development Program of China (Grant No. 2018YFB1106302), and the project (Grant No. 2017WAMC002) sponsored by Anhui Provincial Engineering Research Center of Aluminum Matrix Composites (China).

References

[1] R. Gadow, D. Scherer, Composite coatings with dry lubrication ability on light metal substrates, Surf. Coat. Technol. 151-152 (2002) 471–477.
[2] Y. Madhavi, L. Rama Krishna, N. Narasaiah, Corrosion-fatigue behavior of micro-arc oxidation coated 6061-T6 Al alloy, Int. J. Fatigue 142 (2021).
[3] K. Ma, T. Hu, H. Yang, T. Topping, A. Yousefiani, E.J. Lavernia, J.M. Schoenung, Coupling of dislocations and precipitates: impact on the mechanical behavior of ultrafine grained Al–Zn–Mg alloys, Acta Mater. 103 (2016) 153–164.
[4] X. Peng, Q. Guo, X. Liang, Y. Deng, Y. Gu, G. Xu, Z. Yin, Mechanical properties, corrosion behavior and microstructures of a non-isothermal ageing treated Al-Zn-Mg-Cu alloy, Mater. Sci. Eng. A 688 (2017) 146–154.
[5] Y. Zou, L. Cao, X. Wu, Y. Wang, X. Sun, H. Song, M.J. Couper, Effect of ageing temperature on microstructure, mechanical property and corrosion behavior of aluminum alloy 7085, J. Alloys Compd. 823 (2020).
[6] B. Nie, P. Liu, T. Zhou, Effect of compositions on the quenching sensitivity of 7050 and 7085 alloys, Mater. Sci. Eng. A 667 (2016) 106–114.
[7] S. Liu, Q. Li, H. Lin, L. Sun, T. Long, L. Ye, Y. Deng, Effect of quench-induced precipitation on microstructure and mechanical properties of 7085 aluminum alloy, Mater. Des. 132 (2017) 119–128.
[8] G. Li, W. Jiang, F. Guan, J. Zhu, Z. Zhang, Z. Fan, Microstructure, mechanical properties and corrosion resistance of A356 aluminum/AZ91D magnesium bimetal prepared by a compound casting combined with a novel Ni-Cu composite interlayer, J. Mater. Process. Technol. 288 (2021).
[9] K. Sakata, K. Tagomori, N. Sugiyama, M. Takenouchi, Y. Shinya, K. Morimoto, Y. Suzuki, Development of nanoporous alumina catalyst support by anodic oxidation of thermally and kinetically sprayed aluminum coatings, J. Therm. Spray Technol. 22 (2012) 138–144.
[10] R.T.R. McGrann, D.J. Greving, J.R. Shadley, E.F. Rybicki, T.L. Kruecke, B. E. Bodger, The effect of coating residual stress on the fatigue life of thermal spray-coated steel and aluminum, Surf. Coat. Technol. 108-109 (1998) 59–64.
[11] M.I. Bashir, M. Shafiq, M. Naeem, M. Zaka-ul-Islam, J.C. Díaz-Guillén, C.M. Lopez-Badillo, M. Zakaullah, Enhanced surface properties of aluminum by PVD-TiN coating combined with cathodic cage plasma nitriding, Surf. Coat. Technol. 327 (2017) 59–65.
[12] J. Senf, E. Broszeit, Wear and corrosion protection of aluminum and magnesium alloys using chromium and chromium nitride PVD coatings, Adv. Eng. Mater. 1 (1999) 133–137.
[13] S. Sanjay, K. Baskar, Fabrication of Schottky barrier diodes on clump of gallium nitride nanowires grown by chemical vapour deposition, Appl. Surf. Sci. 456 (2018) 526–531.
[14] K. Liu, Y. Li, J. Wang, In-situ reactive fabrication and effect of phosphorus on microstructure evolution of Ni/Ni–Al intermetallic composite coating by laser cladding, Mater. Des. 105 (2016) 171–178.
[15] T.M. Yue, Y.X. Wu, H.C. Man, Laser surface treatment of aluminium 6013/SiCpcomposite for corrosion resistance enhancement, Surf. Coat. Technol. 114 (1999) 13–18.
[16] Y. Li, Y. Shi, Microstructure and wear resistance of the laser-cladded Al0.8CrFeCoNiCu0.5Bx high-entropy alloy coating on aluminum, Mater. Res. Express 7 (2020).
[17] R. Arrabal, J.M. Mota, A. Criado, A. Pardo, M. Mohedano, E. Matykina, Assessment of duplex coating combining plasma electrolytic oxidation and polymer layer on AZ31 magnesium alloy, Surf. Coat. Technol. 206 (2012) 4692–4703.
[18] K. Dong, Y. Song, D. Shan, E.-H. Han, Corrosion behavior of a self-sealing pore micro-arc oxidation film on AM60 magnesium alloy, Corros. Sci. 100 (2015) 275–283.
[19] H. Duan, K. Du, C. Yan, F. Wang, Electrochemical corrosion behavior of composite coatings of sealed MAO film on magnesium alloy AZ91D, Electrochim. Acta 51 (2006) 2898–2908.
[20] M.W. Urban, D. Davydovich, Y. Yang, T. Demir, Y. Zhang, L. Casabianca, Key-and-lock commodity self-healing copolymers, Science 362 (2018) 220–225.
[21] I. Gurrappa, I.V.S. Yashwanth, The importance of corrosion and the necessity of applying intelligent coatings for its control, in: Intelligent Coatings for Corrosion Control, 2015, pp. 17–58.
[22] S. Hautakangas, H. Schut, N.H. van Dijk, P.E.J. Rivera Díaz del Castillo, S. van der Zwaag, Self-healing of deformation damage in underaged Al–Cu–Mg alloys, Scr. Mater. 58 (2008) 719–722.
[23] S. Manasa, A. Jyothirmayi, T. Siva, S. Sathiyanarayanan, K.V. Gobi, R. Subasri, Effect of inhibitor loading into nanocontainer additives of self-healing corrosion protection coatings on aluminum alloy A356.0, J. Alloys Compd. 726 (2017) 969–977.
[24] T. Wang, J. Du, S. Ye, L. Tan, J. Fu, Triple-stimuli-responsive smart Nanocontainers enhanced self-healing anticorrosion coatings for protection of aluminum alloy, ACS Appl. Mater. Interfaces 11 (2019) 4425–4438.
[25] G. Williams, R. Grace, R.M. Woods, Inhibition of the localized corrosion of mg alloy AZ31 in chloride containing electrolyte, Corrosion 71 (2015) 184–198.
[26] L. Paussa, N.C. Rosero Navarro, D. Bravin, F. Andreatta, A. Lanzutti, M. Aparicio, A. Durán, L. Fedrizzi, ZrO2 sol–gel pre-treatments doped with cerium nitrate for the corrosion protection of AA6060, Prog. Org. Coat. 74 (2012) 311–319.
[27] C.J. Hansen, W. Wu, K.S. Toohey, N.R. Sottos, S.R. White, J.A. Lewis, Self-healing materials with interpenetrating microvascular networks, Adv. Mater. 21 (2009) 4143–4147.
[28] S.A. Kulinich, A.S. Akhtar, D. Susac, P.C. Wong, K.C. Wong, K.A.R. Mitchell, On the growth of conversion chromate coatings on 2024-Al alloy, Appl. Surf. Sci. 253 (2007) 3144–3153.
[29] A. Tiwari, J. Zhu, L.H. Hihara, The development of low-temperature hardening silicone ceramer coatings for the corrosion protection of metals, Surf. Coat. Technol. 202 (2008) 4620–4635.
[30] G. Yoganandan, K. Pradeep Premkumar, J.N. Balaraju, Evaluation of corrosion resistance and self-healing behavior of zirconium–cerium conversion coating developed on AA2024 alloy, Surf. Coat. Technol. 270 (2015) 249–258.
[31] S.R. White, N.R. Sottos, P.H. Geubelle, J.S. Moore, M.R. Kessler, S.R. Sriram, E. N. Brown, S. Viswanathan, Erratum: correction: autonomic healing of polymer composites, Nature 415 (2002) 817.
[32] M.L. Zheludkevich, J. Tedim, C.S.R. Freire, S.C.M. Fernandes, S. Kallip, A. Lisenkov, A. Gandini, M.G.S. Ferreira, Self-healing protective coatings with "green" chitosan based pre-layer reservoir of corrosion inhibitor, J. Mater. Chem. 21 (2011).
[33] I.Z. Ismagilov, R.P. Ekatpure, L.T. Tsykoza, E.V. Matus, E.V. Rebrov, M.H.J.M. de Croon, M.A. Kerzhentsev, J.C. Schouten, Optimization of anodic oxidation and Cu–Cr oxide catalyst preparation on structured aluminum plates processed by electro discharge machining, Catal. Today 105 (2005) 516–528.
[34] H.X. Li, V.S. Rudnev, X.H. Zheng, T.P. Yarovaya, R.G. Song, Characterization of Al2O3 ceramic coatings on 6063 aluminum alloy prepared in borate electrolytes by micro-arc oxidation, J. Alloys Compd. 462 (2008) 99–102.
[35] S. Ji, Y. Weng, Z. Wu, Z. Ma, X. Tian, R.K.Y. Fu, H. Lin, G. Wu, P.K. Chu, F. Pan, Excellent corrosion resistance of P and Fe modified micro-arc oxidation coating on Al alloy, J. Alloys Compd. 710 (2017) 452–459.
[36] A.S. Gnedenkov, S.L. Sinebryukhov, D.V. Mashtalyar, S.V. Gnedenkov, Localized corrosion of the Mg alloys with inhibitor-containing coatings: SVET and SIET studies, Corros. Sci. 102 (2016) 269–278.
[37] D. Liu, E.H. Han, Y. Song, D. Shan, Enhancing the self-healing property by adding the synergetic corrosion inhibitors of Na3PO4 and 2-mercaptobenzothiazole into the coating of Mg alloy, Electrochim. Acta 323 (2019).
[38] K. Aramaki, A self-healing protective film prepared on zinc by treatment in a Ce (NO3)3 solution and modification with Ce(NO3)3, Corros. Sci. 47 (2005) 1285–1298.

[39] R.E. Sykora, L. Deakin, A. Mar, S. Skanthakumar, L. Soderholm, T.E. Albrecht-Schmitt, Isolation of intermediate-valent Ce(III)/Ce(IV) hydrolysis products in the preparation of cerium iodates: electronic and structural aspects of Ce2(IO3)6(OHx) (x ≈ 0 and 0.44), Chem. Mater. 16 (2004) 1343–1349.
[40] E. Paparazzo, G.M. Ingo, N. Zacchetti, X-ray induced reduction effects at CeO2 surfaces: an x-ray photoelectron spectroscopy study, J. Vac. Sci. Technol. A 9 (1991) 1416–1420.
[41] D.D. Sarma, C.N.R. Rao, XPES studies of oxides of second- and third-row transition metals including rare earths, J. Electron Spectrosc. Relat. Phenom. 20 (1980) 25–45.
[42] A. von Richthofen, R. Domnick, Metastable single-phase polycrystalline aluminium oxynitride films grown by MSIP: constitution and structure, Thin Solid Films 283 (1996) 37–44.
[43] A.M. Venezia, R. Bertoncello, G. Deganello, X-ray photoelectron spectroscopy investigation of pumice-supported nickel catalysts, Surf. Interface Anal. 23 (1995) 239–247.
[44] A. Dauscher, L. Hilaire, F. Le Normand, W. Müller, G. Maire, A. Vasquez, Characterization by XPS and XAS of supported Pt/TiO2–CeO2 catalysts, Surf. Interface Anal. 16 (1990) 341–346.
[45] A.J. Aldykiewicz, A.J. Davenport, H.S. Isaacs, Studies of the formation of cerium-rich protective films using X-ray absorption near-edge spectroscopy and rotating disk electrode methods, J. Electrochem. Soc. 143 (2019) 147–154.
[46] C. Zhang, X. Luo, X. Pan, L. Liao, X. Wu, Y. Liu, Self-healing Li-Al layered double hydroxide conversion coating modified with aspartic acid for 6N01 Al alloy, Appl. Surf. Sci. 394 (2017) 275–281.
[47] D. Liu, Y. Song, D. Shan, E.H. Han, Self-healing coatings prepared by loading interphase inhibitors into MAO coating of AM60 Mg alloy, J. Electrochem. Soc. 165 (2018) C412–C421.
[48] R.G. Buchheit, H. Guan, S. Mahajanam, F. Wong, Active corrosion protection and corrosion sensing in chromate-free organic coatings, Prog. Org. Coat. 47 (2003) 174–182.
[49] L. Wen, Y. Wang, Y. Zhou, J.-H. Ouyang, L. Guo, D. Jia, Corrosion evaluation of microarc oxidation coatings formed on 2024 aluminium alloy, Corros. Sci. 52 (2010) 2687–2696.
[50] A.S. Nguyen, N. Pébère, A local electrochemical impedance study of the self-healing properties of waterborne coatings on 2024 aluminium alloy, Electrochim. Acta 222 (2016) 1806–1817.
[51] C.D. Wagner, D.E. Passoja, H.F. Hillery, T.G. Kinisky, H.A. Six, W.T. Jansen, J. A. Taylor, Auger and photoelectron line energy relationships in aluminum–oxygen and silicon–oxygen compounds, J. Vac. Sci. Technol. 21 (1982) 933–944.
[52] B. Kasprzyk-Hordern, Chemistry of alumina, reactions in aqueous solution and its application in water treatment, Adv. Colloid Interf. Sci. 110 (2004) 19–48.